Rescattering photoelectron spectroscopy of heterodiatomic molecules with an analytical returning photoelectron wave packet

Yuta Ito,[1] Misaki Okunishi,[1] Toru Morishita,[2] Oleg I. Tolstikhin,[3] and Kiyoshi Ueda[1]

[1]*Institute of Multidisciplinary Research for Advanced Materials, Tohoku University, 2-1-1 Katahira, Aoba-ku, Sendai-shi 980-8577, Japan*

[2]*Institute for Advanced Science, The University of Electro-Communications, 1-5-1 Chofu-ga-oka, Chofu-shi, Tokyo 182-8585, Japan*

[3]*Moscow Institute of Physics and Technology, Dolgoprudny 141700, Russia*

(Received 6 March 2018; published 23 May 2018)

We present an experimental and theoretical study of photoelectron momentum distributions for nitric oxide (NO) and carbon monoxide (CO) molecules generated by intense linearly polarized laser pulses. It is shown that the measured distributions along the outermost backward rescattering caustic are well reproduced by calculations based on the factorization formula with the analytical returning photoelectron wave packet (RWP) recently derived from the adiabatic theory [T. Morishita and O. I. Tolstikhin, Phys. Rev. A **96**, 053416 (2017)]. The good agreement between the experimental and theoretical results confirms the validity of the theory for molecular targets. We discuss the dependence of the RWP on the scattering angle not taken into account in previous studies. We also discuss its dependence on the orientation of a molecule with respect to the laser field, which reveals a role of depletion of the initial state for the systems and pulses considered.

DOI: 10.1103/PhysRevA.97.053411

I. INTRODUCTION

After the birth of high-intensity ultrashort lasers, various phenomena related to the highly nonlinear response of materials to a strong laser field have been revealed. For instance, high-order harmonic generation [1], nonsequential double ionization [2], and high-order above-threshold ionization [3,4] induced by intense lasers were realized with their high nonlinearity far beyond the perturbation regime. For such phenomena, rescattering processes play a key role [5], where an electron released from an atom or a molecule returns back driven by the oscillating laser field and is scattered by the parent ion. It is recognized that experimental observables resulting from rescattering-based phenomena contain valuable information on the target structure and can provide ultrafast imaging of atoms and molecules on the attosecond timescale due to the subcycle nature of the rescattering process. In particular, laser-induced electron diffraction, utilizing the elastically rescattered electrons, has been proposed theoretically [6] for extracting molecular geometry information and demonstrated in the pioneering experiment [7].

A real breakthrough in the subject came with the theoretical development of the factorization formula for strong-field photoelectron momentum distributions (PEMDs). The formula was first inferred from numerical calculations [8] and then derived analytically for several models under different assumptions [9–11]. It states that PEMDs near the high-energy cutoff can be factorized into the differential cross section (DCS) for elastic scattering of a photoelectron on the parent ion and a returning photoelectron wave packet (RWP). Thus, using this formula, one can extract DCSs from experimentally measured PEMDs, provided that the RWP is known. Experimental verification of the factorization and the DCS extraction procedure was reported for rare gas atoms [12,13]. Later, the same procedure was applied to linear [14] and planar [15] molecules. Once the electron-ion DCS is extracted from experimental data, by comparing it with the theoretical DCS one can obtain related target structure information such as atomic charge density [16,17] and molecular geometry [18–23]. In most of the applications to molecules [18–21], an independent atom model [24] was employed for calculating the DCS, which is justified by the high energy of rescattered photoelectrons for the long wavelength pulses used. In recent studies [22,23], *ab initio* calculations of DCSs were performed, since relatively lower rescattering energy was targeted with shorter wavelength pulses and the independent atom model fails in this case.

However, despite the success of the method demonstrated in Refs. [12–23], the target structure extraction procedure employed therein relied on approximations which limited its accuracy. Following the original paper [8], in all these studies the line in the photoelectron momentum space, from which the experimental information should be extracted, was approximated by a circle with a constant incident momentum and the RWP along this line was assumed to be independent of the scattering angle. Under these approximations, one can extract the DCS without knowing the RWP, but only up to an unknown incident-momentum-dependent factor. An additional ambiguity is caused by the fact that the line was often chosen in an *ad hoc* way somewhere at intermediate photoelectron energies [17–23]. A different approach to the extraction procedure based on the factorization formula derived from the adiabatic theory [25] was demonstrated in Ref. [26]. The adiabatic theory shows that the factorization holds near the outermost backward rescattering caustic in the photoelectron momentum space, where long and short rescattering trajectories originating from the same half-cycle of the laser field coalesce, and yields an analytical form of the scattering angle and incident-momentum-dependent RWP. A preliminary version of the formula presented in Ref. [26] was

generalized, corrected in several important ways, including the description of a quantum shift of the caustic, and validated quantitatively by calculations for several atomic targets treated within the single-active-electron (SAE) approximation in a comprehensive theoretical study [27]. The knowledge of the position and shape of the caustic, where the factorization formula should be applied, and the explicit analytical form of the RWP enables one to eliminate the approximations and ambiguities of previous approaches. In Ref. [26], the theory was applied to extracting DCSs from experimental PEMDs for rare gas atoms generated by few-cycle pulses with carrier-envelope phase control. One of the next challenges is to apply it to molecular targets.

In this paper, we present an experimental and theoretical study of PEMDs for heterodiatomic molecules of nitric oxide (NO) and carbon monoxide (CO). In the theoretical analysis, we consistently employ the SAE approximation with realistic molecular potentials for calculating both the DCS and target-dependent factors in the RWP. We note that the SAE approximation for DCS is by far more accurate than the independent atom model [18–21] and at the same time more feasible computationally than *ab initio* scattering calculations [22,23]. The results are plugged into the factorization formula derived in Ref. [27], averaged over the molecular orientation, and compared with the experimental PEMDs. The NO molecule is a radical species, its singly charged ion NO^+ has a stable electronic configuration similar to that of N_2, and it is expected that the only electron in its highest occupied molecular orbital (HOMO) should be well described by the SAE approximation. Thus, NO is an ideal system for critical tests of SAE-based theoretical predictions. In contrast, CO has paired electrons in the closed-shell HOMO, which may affect the ionization and rescattering dynamics. Indeed, there are several discussions on multielectron effects in strong-field ionization of CO [28–30]. In addition, NO and CO have very different electronic properties, such as the ionization potential, the permanent dipole moment, the nodal structure of the HOMO, and so on. A comparative study of these two molecules is a good test for checking the validity of the theory and providing foresight for further applications to larger systems.

The paper is organized as follows. In Sec. II, we briefly outline the experimental setup used to measure the PEMDs for NO and CO molecules generated by intense near-infrared laser pulses. In Sec. III, we describe our theoretical procedure based on the factorization formula with the analytical RWP derived in Ref. [27] and the SAE approximation. In Sec. IV, we thoroughly compare the experimental and theoretical PEMDs along the backward rescattering caustic in a range of scattering angles and incident momenta for different laser wavelengths and intensities. We illustrate the importance of taking into account the dependence of the RWP on the scattering angle. We also discuss its dependence on the orientation of a molecule with respect to the ionizing field. Section V concludes the paper.

II. EXPERIMENT

The experimental setup is almost the same as that in our previous papers [21,23]. A Ti:sapphire laser system (800 nm, 100 fs, 1.5 mJ/pulse, 1 kHz) was used to pump an optical parametric amplifier, obtaining the signal and idler outputs separated by dichroic mirrors. Those outputs, whose wavelength was set to 1300 nm for the signal and 1650 nm for the idler, induced target ionization and photoelectron rescattering. Sample gas was supplied as an effusive molecular beam in an ultrahigh vacuum chamber, on which the laser beam was focused by a concave mirror ($f = 75$ mm). The time-of-flight of electrons through a 264-mm-length field-free drift tube was measured to obtain their momentum. The polarization direction of the laser beam was swept with a broadband half-wave plate. We thus measure the density of events in three-dimensional photoelectron momentum space, which up to a constant normalization factor coincides with the three-dimensional PEMD. The measured PEMDs are axially symmetric about the polarization axis. Below we consider their two-dimensional cuts by a plain passing through the polarization axis (see Fig. 1).

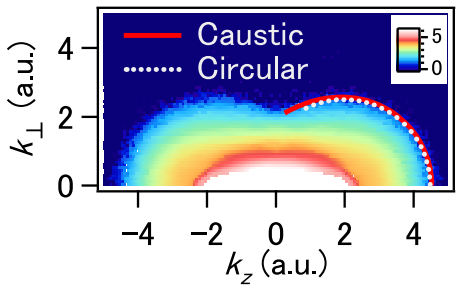

FIG. 1. Experimental PEMD for NO molecules in a 1650-nm laser field displayed on a logarithmic scale (arbitrary units) with false colors. The PEMD is axially symmetric about the polarization axis k_z; the figure shows its two-dimensional cut by a plain passing through this axis. The solid (red) line shows the outermost quantum caustic $\tilde{\mathbf{k}}(\theta)$, Eqs. (1), determined by the effective peak field amplitude $\bar{F}_0 = 0.055$ a.u., and the dotted (white) line shows the circular approximation to the caustic. The scattering angle θ varies along the lines in the interval $60^\circ \leqslant \theta \leqslant 180^\circ$.

III. THEORY

We assume that the laser pulse is linearly polarized along the z axis and has a Gaussian envelope, so the electric field is $\mathbf{F}(t) = F(t)\mathbf{e}_z$, with $F(t) = F_0 \exp[-(2t/T)^2]\cos\omega t$, where F_0 is the peak field amplitude, ω is the laser frequency, and $\sqrt{\ln 2}\,T$ is the full width at half maximum of the pulse. The orientation of a molecule is described by the Euler angles (α,β,γ) defining a rotation from the laboratory frame to the molecular frame [31]. For the present case of heterodiatomic molecules, β is the angle between the polarization vector $\mathbf{e}_z$ and the oriented internuclear axis, α describes the rotation of the internuclear axis about the polarization axis, and we set $\gamma = 0$. The photoelectron momentum is denoted by $\mathbf{k} = (k_x,k_y,k_z)$, where $k_x = k_\perp \cos\varphi_k$ and $k_y = k_\perp \sin\varphi_k$. The experimental PEMD is axially symmetric about the k_z axis, that is, it does not depend on φ_k, because of averaging over random orientations of molecules, so we consider it in a half-plane $\varphi_k = \text{const}$ with coordinates $(k_\perp,k_z)$ (see Fig. 1). We first discuss the theory for a molecule with fixed orientation defined by the angles α and β, and then we perform the averaging.

A rescattering event is characterized by scattering angles $\Omega = (\theta,\varphi)$ measured relative to the direction of the incident

momentum. In the adiabatic regime [25], the incident momentum of a photoelectron arriving for rescattering is directed along the polarization axis, so we identify the azimuthal scattering angle φ with φ_k. Long and short rescattering trajectories originating from the same half-cycle of the laser field and contributing to the same final photoelectron momentum may coalesce. A surface in the photoelectron momentum space where this happens is called a backward rescattering caustic [27]. The caustic is a surface of revolution about the k_z axis. We parametrize it by the scattering angles Ω. Its section by the plane $(k_\perp,k_z)$ is a line which we parametrize by θ and denote by $\mathbf{k}(\theta)$. The caustic is a classical object completely determined by the field $F(t)$, its explicit form is defined in Ref. [27]. Let $t_i(\theta)$ and $t_r(\theta)$ denote the moments of ionization and rescattering at the caustic, respectively; in the following, for brevity, we omit their argument. For a many-cycle pulse, there are many caustics produced by pairs of long and short rescattering trajectories originating from the different cycles. We are interested only in the outermost classical caustic for which ionization and rescattering occur near the peak of the pulse at $t = 0$. The corresponding quantum caustic is also a surface of revolution about the k_z axis which crosses the plane $(k_\perp,k_z)$ along the line [27]

$$\tilde{\mathbf{k}}(\theta) = \mathbf{k}(\theta) + q(\theta)\boldsymbol{\nu}(\theta), \tag{1a}$$

$$q(\theta) = \frac{-E_\beta(t_i)}{(t_r - t_i)|F(t_i)|}. \tag{1b}$$

The second term in Eq. (1a) describes a shift in the direction of the vector $\boldsymbol{\nu}(\theta)$, giving the external unit normal to $\mathbf{k}(\theta)$. The shift has a quantum origin, its value (1b) depends on the energy $E_\beta(t)$ of the Siegert state emerging from the unperturbed ionizing molecular orbital in the presence of a static electric field equal to the instantaneous laser field $F(t)$ [32]. Note that the Siegert energy is complex; its real part accounts for the Stark shift of the state and its imaginary part defines the instantaneous tunneling ionization rate $\Gamma_\beta(t) = -2\,\mathrm{Im}\,E_\beta(t)$. For diatomic molecules, this energy depends on β, which is indicated by the subscript, but does not depend on α. We consider the PEMD only at the quantum caustic. For a molecule with fixed orientation this PEMD is denoted by $P(\Omega;\alpha,\beta)$. In the adiabatic approximation [25] it takes the factorized form [27]

$$P(\Omega;\alpha,\beta) = |f_\beta(u_f(\theta),\Omega_\alpha)|^2 W_\beta(\theta). \tag{2}$$

Here $f_\beta(k,\Omega)$ is the scattering amplitude defining the DCS $d\sigma_\beta/d\Omega = |f_\beta(k,\Omega)|^2$ for elastic scattering of an electron with incident momentum $k\mathbf{e}_z$ by the molecular ion with the orientation angles $\alpha = 0$ and β, $u_f(\theta)$ is the incident momentum at the classical caustic $\mathbf{k}(\theta)$, and the notation $\Omega_\alpha = (\theta,\varphi-\alpha)$ indicates that for a nonzero α the DCS depends only on the difference between the angles φ and α. The second factor in Eq. (2) is the RWP taken at the quantum caustic $\tilde{\mathbf{k}}(\theta)$; its explicit form is given by

$$W_\beta(\theta) = |\mathrm{Ai}(0)|^2 \left|\frac{2}{S_r'''(\theta)}\right|^{2/3} \frac{4\pi^2|A_\beta(t_i)|^2}{(t_r-t_i)^3|F(t_i)|} \times \exp\left[-\int_{-\infty}^{t_i}\Gamma_\beta(t)dt\right], \tag{3}$$

where $\mathrm{Ai}(0) \approx 0.355$ is the Airy function at zero argument and

$$S_r'''(\theta) = u_f(\theta)\left[2\dot{F}(t_r)\sin^2(\theta/2) - \frac{3F(t_r)}{t_r-t_i} - \frac{3u_f(\theta)}{(t_r-t_i)^2} - \frac{u_f^2(\theta)}{(t_r-t_i)^3F(t_i)}\right]. \tag{4}$$

Here $A_\beta(t)$ is another property of the Siegert state in the instantaneous laser field $F(t)$, namely, the transverse momentum distribution (TMD) amplitude [33] taken at zero transverse momentum. This quantity also depends on β, but is independent of α. The last exponential factor in Eq. (3), where $\Gamma_\beta(t)$ is the ionization rate introduced above, describes depletion of the initial state. Note that the RWP (3) depends on neither φ nor α, so the PEMD (2) depends only on the difference between these angles through the DCS. To implement the factorization formula (2), one needs to calculate the characteristics of rescattering at the classical caustic t_i, t_r, and $u_f(\theta)$, which are completely determined by the function $F(t)$, and the molecular properties $f_\beta(k,\Omega)$, $E_\beta(t)$, $\Gamma_\beta(t)$, and $A_\beta(t)$.

To evaluate the molecular properties, we employ the SAE approximation with a molecular potential modeled by the sum of two screened Coulomb potentials with effective charges:

$$V(\mathbf{r}) = -\frac{Z_1(r_1)}{r_1} - \frac{Z_2(r_2)}{r_2}, \tag{5}$$

where $r_1 = |\mathbf{r} + \mathbf{R}/2|$ and $r_2 = |\mathbf{r} - \mathbf{R}/2|$ are the distances from the active electron to the nuclei located at $\pm\mathbf{R}/2$. For our purposes, it is sufficient to consider the case $\alpha = 0$, when the molecule lies in the (x,z) plane of the laboratory frame and the internuclear vector is given by $\mathbf{R} = (R\sin\beta, 0, R\cos\beta)$, where R is the equilibrium internuclear distance in the molecule. We define the effective charges $Z_i(r)$, $i = 1$ and 2, by [34]

$$Z_i(r) = a_i - (b_i - 1)\{1 - [(v_i/u_i)(e^{u_i r} - 1) + 1]^{-1}\}. \tag{6}$$

Here $a_i = Z_i(0)$ is the nuclear charge for the corresponding atom in the molecule. The other parameters are chosen in such a way that some important properties of the SAE potential (5) and a selected bound state in it representing the HOMO of the molecule coincide with their values in the Hartree-Fock (HF) method. The HF values of the properties are calculated using the grid-based HF program described in Ref. [35]. We note that this program yields exact HF results, in contrast to basis-based programs commonly used in quantum chemistry calculations, whose results depend on the basis. We require that the potential satisfy

$$V(\mathbf{r})|_{r\to\infty} = -\frac{1}{r} - \frac{\mathbf{Dn}}{r^2} + O(r^{-3}), \tag{7}$$

where $\mathbf{D} = D\mathbf{R}/R$ is the HF value of the total dipole moment of the parent molecular ion and $\mathbf{n} = \mathbf{r}/r$. Equation (7) amounts to two conditions, $a_1 - b_1 + a_2 - b_2 + 2 = 1$ and $(a_2 - b_2 - a_1 + b_1)R/2 = D$, which can be satisfied by adjusting the two parameters b_i. The remaining parameters u_i and v_i are chosen by minimizing their deviations from the corresponding atomic values tabulated in Ref. [34] while maintaining the energy E_0 and the dipole moment μ_0 of the bound state representing the HOMO of the neutral molecule equal to their HF values for

TABLE I. Characteristics (in atomic units) of the two molecules considered within the SAE approximation. R is the equilibrium internuclear distance; a_i, b_i, u_i, and v_i are the parameters defining the SAE potential (5), with $i = 1$ referring to N in NO and to C in CO and $i = 2$ in both cases referring to O; D is the total dipole moment of the parent molecular ion; E_0 is the energy of the HOMO; and μ_0 is the dipole moment of the HOMO in the geometrical center frame. The values of D, E_0, and μ_0 are calculated for the given R using the grid-based Hartree-Fock program described in Ref. [35]. The parameters of the potential (5) are adjusted to reproduce the Hartree-Fock values of the coefficient D in Eq. (7) and the energy E_0 and the dipole moment μ_0 of the bound state representing the HOMO.

Molecule	R	a_1	b_1	u_1	v_1	a_2	b_2	u_2	v_2	D	E_0	μ_0
NO	2.1747	7	7.3656	2.1382	1.1360	8	8.6344	2.1107	1.2775	−0.292	−0.4117	0.462
CO	2.1320	6	6.0215	2.2136	1.0806	8	8.9785	2.0269	1.2709	−1.020	−0.5549	1.565

the HOMO. The thus obtained parameters defining the SAE potentials for NO and CO are listed in Table I.

To construct the unperturbed initial state, we diagonalize the field-free SAE Hamiltonian with the potential (5) for $\beta = 0$ in prolate spheroidal coordinates and select the eigenstate which has the same symmetry and nodal structure as the HOMO of the molecule under consideration. The HOMO of NO is a π state having one nodal surface transverse to the internuclear axis, and the HOMO of CO is a σ state having no nodal surfaces. The Siegert energy of the state in Eq. (1b) is approximated by the linear Stark-shifted energy $E_\beta(t) = E_0 - \mu_0 F(t)\cos\beta$. Under this approximation the caustic (1) becomes real, its shape calculated for particular pulse and molecule is illustrated by the solid line in Fig. 1. The ionization rate and the TMD amplitude are evaluated within the weak-field asymptotic theory [36] using

$$\Gamma_\beta(t) = \left[|G_{00}(\beta)|^2 + \frac{F}{2\varkappa^2}|G_{01}(\beta)|^2\right] W_{00}(F) \tag{8}$$

and

$$|A_\beta(t)|^2 = \frac{4\pi\varkappa}{F}|G_{00}(\beta)|^2 W_{00}(F), \tag{9}$$

where $F = |F(t)|$; $\varkappa = \sqrt{-2E_0}$; $G_{00}(\beta)$ and $G_{01}(\beta)$ are structure factors for the dominant and next-to-the-dominant ionization channels, respectively, defined in terms of the unperturbed ionizing orbital in Ref. [37]; and

$$W_{00}(F) = \frac{\varkappa}{2}\left(\frac{4\varkappa^2}{F}\right)^{2/\varkappa-1} \exp\left(-\frac{2\varkappa^3}{3F}\right) \tag{10}$$

is the field factor. Note that the structure factors for NO and CO obtained in the present calculations within the SAE approximation turn out to be very close to the ones obtained for the HOMO of these molecules in the HF method [38]. Note also that there are two degenerate π states of NO, one of which π^+ is even and the other π^- is odd under the reflection $y \to -y$ [38]. Only the π^+ state contributes to rescattering; the π^- state does not contribute, because the TMD amplitude for this state has a node at zero transverse momentum, reflecting a node of the orbital.

The scattering amplitude $f_\beta(k,\Omega)$ is consistently calculated within the same SAE approximation. To this end, we solve the time-independent Schrödinger equation with the potential (5) supplemented by asymptotic boundary conditions for scattering states in spherical coordinates using the slow variable discretization method [39] in combination with the R-matrix propagation technique [40]. The radius is treated as the adiabatic parameter of the method, and spherical harmonics and Legendre polynomials are used as basis sets in the angular and radial coordinates, respectively. This approach has proven to be very efficient and accurate in scattering calculations for various three-body systems [41,42] as well as in calculations of molecular Siegert states [32,33]. Note that it is based on a single-center expansion. Neither this expansion nor computational technologies [39,40] used to implement it rely on any particular symmetry of the potential, which means that the approach can be applied to polyatomic molecules, provided that a reasonable SAE potential is available.

The theoretical procedure described above yields the PEMD (2) for a fixed orientation of the molecule. In order to compare the results with the experimental PEMD measured for randomly oriented molecules, we should average Eq. (2) over the orientation angles α and β. Since the PEMD (2) depends only on the difference $\varphi - \alpha$, the integration over α amounts to that over φ. We thus obtain

$$S(\theta) = \frac{1}{4\pi}\int_0^{2\pi}\int_0^{\pi} P(\Omega;\alpha,\beta)\sin\beta d\beta d\alpha \tag{11a}$$

$$= \frac{1}{4\pi}\int_0^{2\pi}\int_0^{\pi} |f_\beta(u_f(\theta),\Omega)|^2 W_\beta(\theta)\sin\beta d\beta d\varphi. \tag{11b}$$

The function $S(\theta)$ is to be compared with the experimental results.

In addition, for comparison, we consider an approach introduced in Ref. [8] and used in previous studies [12–23]. In this approach, the caustic is approximated by a circle with constant incident momentum equal to $u_f(\theta = 180^\circ)$ and the RWP is assumed to be independent of θ. The circular approximation to the caustic is illustrated by the dotted line in Fig. 1. Within this approach, the experimental results are described by the orientation-averaged DCS weighted with the ionization rate:

$$X(\theta) = \frac{\int_0^{2\pi}\int_0^{\pi} |f_\beta(u_f(\theta),\Omega)|^2 |G_{00}(\beta)|^2 \sin\beta d\beta d\varphi}{2\pi\int_0^{\pi}|G_{00}(\beta)|^2\sin\beta d\beta}. \tag{12}$$

Note that this quantity lacks an absolute normalization factor, in contrast to the orientation-averaged PEMD (11).

IV. RESULTS AND DISCUSSION

An example of experimentally measured PEMD for NO at 1650 nm is presented in Fig. 1. Since a focused laser beam is used to ionize the target molecules, a broad range of laser intensities contribute to the PEMD due to the laser focal volume effect [43,44]. However, only the central part of the focal volume, which corresponds to the peak laser intensity, contributes to the PEMD near the outermost caustic. In order

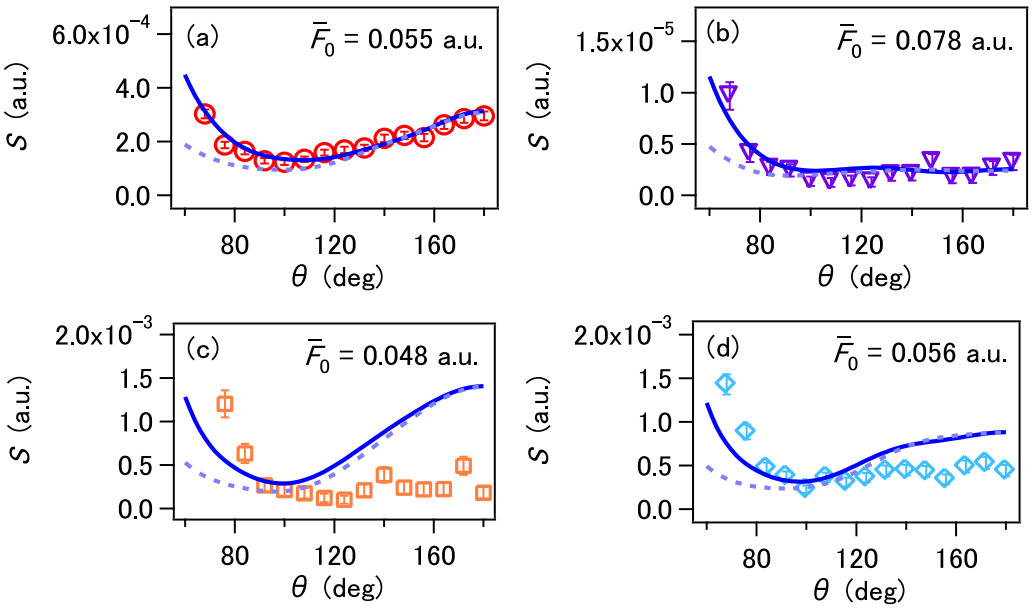

FIG. 2. Experimental (symbols) and theoretical [solid lines, Eq. (11)] PEMDs $S(\theta)$ as functions of the scattering angle θ along the outermost quantum caustic $\tilde{\mathbf{k}}(\theta)$ for NO. The caustic is determined by the effective peak field amplitude (a) $\bar{F}_0 = 0.055$ a.u. ($u_f = 2.5$ a.u.) at 1650 nm, (b) $\bar{F}_0 = 0.078$ a.u. ($u_f = 3.5$ a.u.) at 1650 nm, (c) $\bar{F}_0 = 0.048$ a.u. ($u_f = 1.7$ a.u.) at 1300 nm, and (d) $\bar{F}_0 = 0.056$ a.u. ($u_f = 2.0$ a.u.) at 1300 nm. Dashed lines present orientation-averaged DCSs $X(\theta)$, Eq. (12), which corresponds to the circular approximation with a constant RWP. In each panel, the function $X(\theta)$ is multiplied by a constant factor to bring its value in coincidence with the theoretical curve $S(\theta)$ at $\theta = 180^\circ$.

to extract the experimental $S(\theta)$ as a function of the scattering angle θ along the caustic, we focus on the region near the high-energy edge of the measured PEMD. In the present work, we find the theoretical peak field amplitude F_0 such that the corresponding caustic $\tilde{\mathbf{k}}(\theta)$ at $\theta = 180^\circ$ crosses the k_z axis at the point where the experimental yield drops by 3–4 orders of magnitude compared to the onset of the plateau at smaller k_z (see Fig. 1). We call the result the effective peak field amplitude and denote it by $\bar{F}_0$. For the experimental PEMD shown in Fig. 1 we obtain $\bar{F}_0 = 0.055$ a.u.; the corresponding caustic $\tilde{\mathbf{k}}(\theta)$ and the circular approximation to it are shown by solid (red) and dotted (white) lines, respectively, in the interval of scattering angles $60^\circ \leqslant \theta \leqslant 180^\circ$. Note that although the lines lie close to each other, the rates of variation of θ along them are different, which results in the difference of their lengths. Also note that the difference in the shapes of the lines becomes more pronounced at smaller θ.

In the following, we compare experimental $S(\theta)$ extracted from the measured PEMDs with theoretical results calculated using Eq. (11) and with orientation-averaged DCSs $X(\theta)$ given by Eq. (12). It is noted that to extract the PEMDs along the caustic at one laser intensity, a Jacobian from $(k_\perp, k_z)$ to (F, θ) is taken into account, because the caustic is a function of laser intensity (F). The absolute value of the theoretical $S(\theta)$ is defined by Eq. (11). The experimental results lack a common factor. We normalize them by requiring that the integrals of experimental and theoretical $S(\theta)$ over the interval $60^\circ \leqslant \theta \leqslant 180^\circ$ considered in the figures have the same values. For the comparison with $S(\theta)$, the quantity $X(\theta)$ also must be normalized. We do this by requiring that $X(\theta)$ coincides with the theoretical $S(\theta)$ at $\theta = 180^\circ$. These normalizations are used in all the figures shown below.

Experimental $S(\theta)$ values for NO molecules generated by four pulses with two different intensities at each of the wavelengths 1650 and 1300 nm are shown in Fig. 2 by symbols. The corresponding theoretical results obtained from Eq. (11) are shown by solid (blue) lines. The effective peak field amplitude $\bar{F}_0$ for each pulse is indicated in the figure. An additional useful characteristic of the pulse, the incident momentum for the backward rescattering $u_f = u_f(\theta = 180^\circ)$, is also given in the caption to the figure. One can see a fairly good agreement between experimental and theoretical results in the broad range of θ, particularly for both intensities at the longer wavelength 1650 nm in Figs. 2(a) and 2(b). From the standpoint of the adiabatic theory [25], the factorization formula (2) becomes more accurate as the wavelength grows for a given pulse intensity, and this is confirmed by calculations for atomic targets [27]. The present results also confirm this trend. Indeed, the theoretical curve clearly approaches the experimental points as one moves from 1300 nm in Fig. 2(d) to 1650 nm in Fig. 2(a) for almost the same intensity defined by the effective peak field amplitude $\bar{F}_0$. Furthermore, Eq. (2) should work better as the intensity grows for a given wavelength, as confirmed by calculations for atomic targets [27]. This is again confirmed by the results in Figs. 2(c) and 2(d). The level of agreement seen in Fig. 2 signifies an experimental confirmation of the factorization formula (2) for molecular targets. We can also conclude that its present implementation based on the SAE approximation with a potential reproducing some important properties of the ionizing orbital calculated by the HF method well describes the ionization dynamics of the unpaired active electron in NO, as expected. For comparison, the orientation-averaged DCSs $X(\theta)$ obtained from Eq. (12) are also shown in Fig. 2 by dashed lines. One can clearly see that in

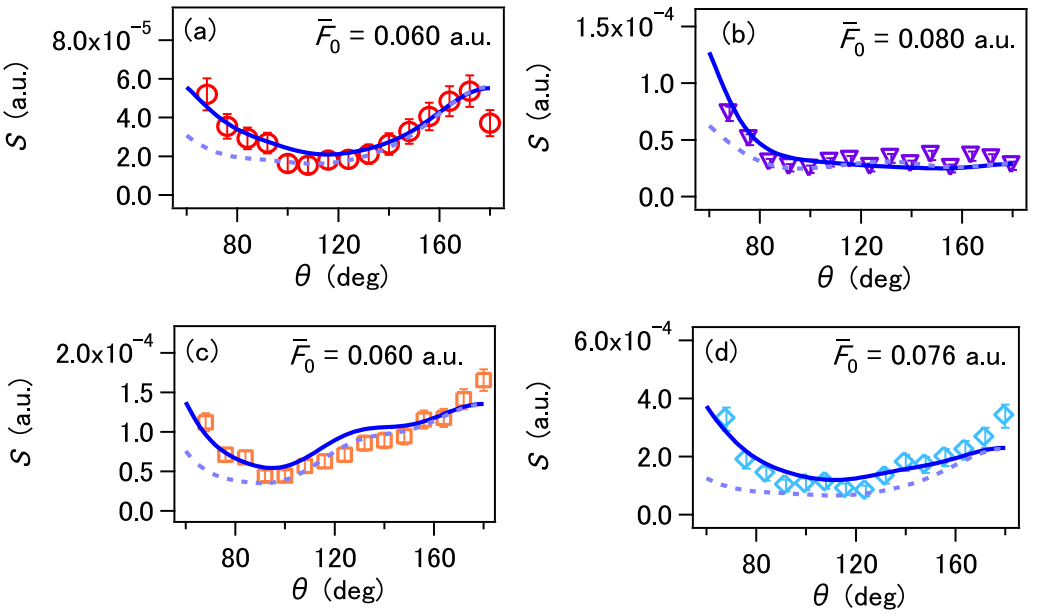

FIG. 3. Similar to Fig. 2, but for CO. The caustic is determined by the effective peak field amplitude (a) $\bar{F}_0 = 0.060$ a.u. ($u_f = 2.7$ a.u.) at 1650 nm, (b) $\bar{F}_0 = 0.080$ a.u. ($u_f = 3.6$ a.u.) at 1650 nm, (c) $\bar{F}_0 = 0.060$ a.u. ($u_f = 2.1$ a.u.) at 1300 nm, and (d) $\bar{F}_0 = 0.076$ a.u. ($u_f = 2.7$ a.u.) at 1300 nm.

all the cases the dashed line lies farther from the experimental results than the theoretical solid line, especially at smaller θ. This indicates that the analytical scattering-angle-dependent RWP (3) derived from the adiabatic theory [25] plays an important role in the description of the rescattering process.

Figure 3 presents similar results for CO molecules. In this case, a very good agreement between experimental and theoretical $S(\theta)$ is seen even for the shorter wavelength 1300 nm, and the agreement becomes better for the longer wavelength 1650 nm, in accordance with the adiabatic theory. Since CO has a larger ionization potential compared to NO (see Table I), the adiabatic approximation in the description of strong-field ionization holds for CO better than for NO under similar laser parameters [25]. This partially explains why the agreement for CO is better than that for NO. It is worth noting that the DCS factors in the factorization formula (2) for the pulses shown in Figs. 3(a) and 3(d) are the same because of the same value of $u_f = 2.7$, and hence the small but non-negligible difference in the shapes of the theoretical curves $S(\theta)$ for these two pulses stems solely from the RWPs. The reproduction of the experimental results in such cases is another illustration of the importance of having the analytical RWP for describing the rescattering process. From the good agreement seen in Fig. 3 we can conclude that the SAE approximation works for the description of the ionization dynamics of a paired electron in the HOMO of CO as well as it does for an unpaired electron in the HOMO of NO. The circular approximation with a constant RWP shown by dashed lines is again consistently worse than the results of the adiabatic theory.

Let us discuss the structure of the RWP (3) in more detail. The RWPs for NO and CO calculated for two particular pulses shown in Figs. 2(b) and 3(b), respectively, are displayed as functions of the scattering angle θ and the molecular orientation angle β in Fig. 4. For each molecule we have chosen

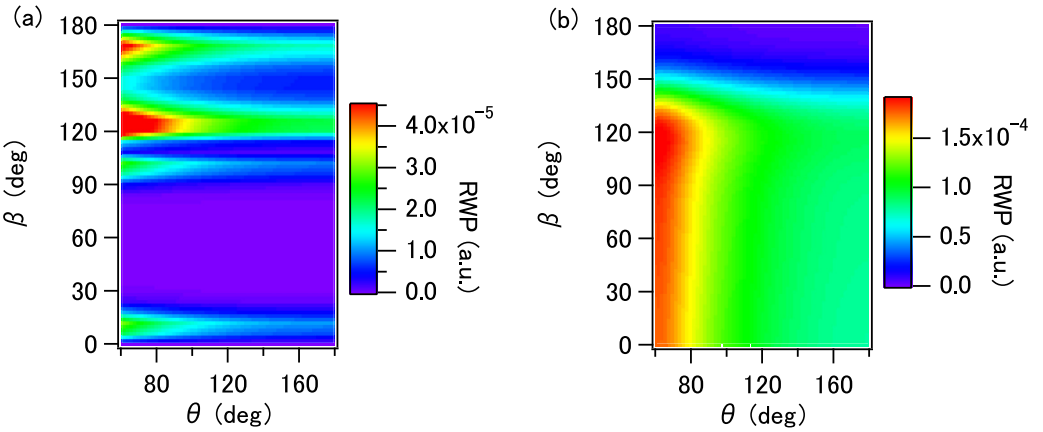

FIG. 4. Theoretical RWP $W_\beta(\theta)$, Eq. (3), for (a) NO under a pulse with $\bar{F}_0 = 0.078$ a.u. at 1650 nm, as in Fig. 2(b), and (b) CO under a pulse with $\bar{F}_0 = 0.080$ a.u. at 1650 nm, as in Fig. 3(b), as a function of the scattering angle θ and the molecular orientation angle β.

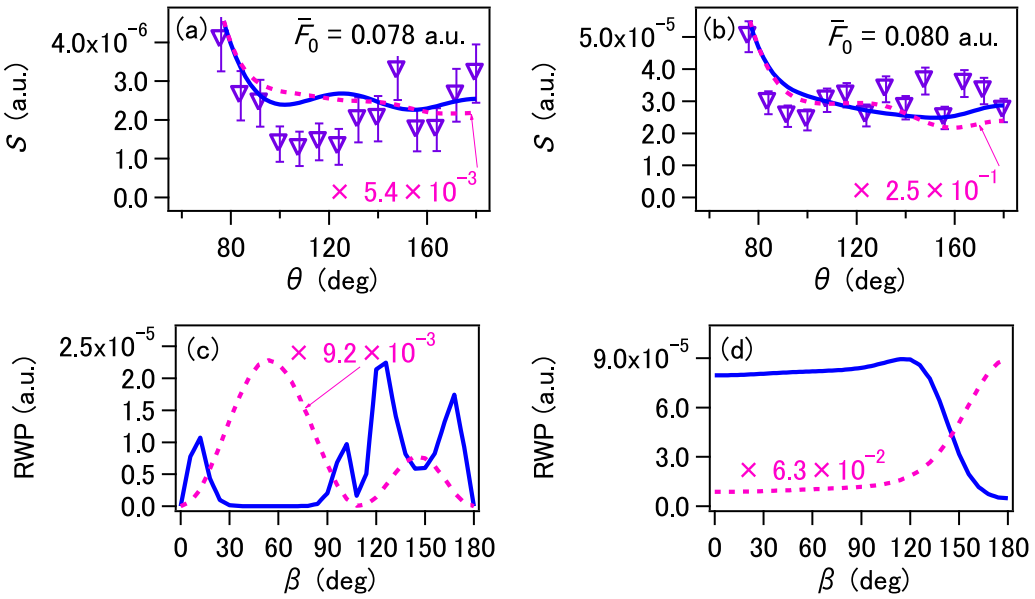

FIG. 5. The upper panels show experimental (symbols) and theoretical [solid lines, Eq. (11)] PEMDs $S(\theta)$ as functions of the scattering angle θ along the outermost quantum caustic $\tilde{\mathbf{k}}(\theta)$ for (a) NO under a pulse with $\bar{F}_0 = 0.078$ a.u. and (b) CO under a pulse with $\bar{F}_0 = 0.080$ a.u., in both cases at 1650 nm. These results are the same as those in Figs. 2(b) and 3(b), but are shown on a finer vertical scale. The lower panels show the RWPs $W_\beta(\theta)$, Eq. (3), for the same pulses used to calculate the theoretical $S(\theta)$ for (c) NO, as in Fig. 4(a), and (d) CO, as in Fig. 4(b), as functions of the molecular orientation angle β at the fixed scattering angle $\theta = 180°$. In each panel, the solid (blue) line shows the full theoretical results including the depletion factor in Eq. (3), and the dashed (magenta) line shows the results obtained by omitting this factor.

a pulse with the higher intensity at the longer wavelength. On the one hand, considering the dependence on θ for a fixed β, for both molecules $W_\beta(\theta)$ monotonically grows as θ decreases. The growth is mainly caused by the factor $S_r'''(\theta)$ in Eq. (3) given by Eq. (4), which is completely determined by the field $F(t)$ and does not depend on the target. This explains the difference between $S(\theta)$ and the normalized $X(\theta)$ seen in Figs. 2 and 3, namely, the fact that $S(\theta)$ becomes larger than $X(\theta)$ at smaller θ. On the other hand, the dependence of $W_\beta(\theta)$ on β for a fixed θ is strongly affected by the target. This dependence in Eq. (3) is caused by the TMD amplitude $A_\beta(t)$ and the exponential depletion factor determined by the ionization rate $\Gamma_\beta(t)$. As can be seen from Eqs. (8) and (9), these factors reflect the structure of the ionizing orbital, and hence are different for the two molecules. To obtain more insight into the dependence on β, we have recalculated the RWPs shown in Fig. 4 by omitting the depletion factor. The depletion-free RWPs as functions of β at $\theta = 180°$ are compared with the full RWPs including the depletion factor in Figs. 5(c) and 5(d). The dependence on β of the depletion-free RWPs is determined by the TMD amplitude squared $|A_\beta(\theta)|^2$ in Eq. (3), which in turn is determined by the structure factor $|G_{00}(\beta)|^2$ for the ionizing orbital in Eq. (9). Thus, two peaks at $\beta \approx 60°$ and $150°$ and a node at $\beta \approx 110°$ for NO in Fig. 5(c) and a peak at $\beta \approx 180°$ for CO in Fig. 5(d) reflect the angular dependence of their HOMOs in the asymptotic region multiplied by a dipole factor [36]. A gross effect of the inclusion of the depletion factor in Eq. (3) for the present pulses and molecules consists of the decrease of the overall magnitude of the RWPs by a factor of $\sim 10^2$. However, in addition to this, the depletion factor considerably modifies the dependence of the RWPs on β, as can be seen by comparing the solid and dashed lines in Figs. 5(c) and 5(d). The depletion factor is smaller at molecular orientations corresponding to larger ionization rates. Such orientations are represented by peaks in the dashed lines. These peaks turn into dips in the solid lines after the depletion factor is taken into account, which is a rather counterintuitive feature. In Figs. 5(a) and 5(b), the PEMDs calculated using the RWPs with and without the depletion factor in Eq. (3) are shown by solid and dashed lines, respectively. It is seen that a wavy structure in the experimental $S(\theta)$ for NO in Fig. 5(a) is qualitatively described by the above counterintuitive β dependence of the RWP with depletion, while the RWP without depletion does not reproduce this feature. For the CO molecule in Fig. 5(b), the effect of depletion on the shape of $S(\theta)$ is smaller, although its effect on the RWP is also very large, as seen in Fig. 5(d).

To close this discussion, let us note the following. One should not expect that SAE-based theoretical predictions can perfectly reproduce experimental results for many-electron targets. Instead, such predictions should be used as a reference: the difference between them and experimental results under conditions of validity of the adiabatic approximation should be attributed to many-electron effects. This could refer to many-electron effects in the rescattering process, e.g., resonances in elastic scattering caused by excitation of doubly excited states, but also to effects caused by tunneling ionization from inner molecular orbitals. The quantitative theoretical procedure demonstrated above, which is free from approximations of previous approaches, can enable one to detect such many-electron effects in PEMDs.

V. CONCLUSION

We measured PEMDs for heterodiatomic NO and CO molecules induced by 100-fs intense near-infrared (1650 and 1300 nm) laser pulses with different intensities. We compared

the PEMDs along the outermost quantum caustic with theoretical predictions obtained using the factorization formula (2) with the analytical scattering-angle-dependent RWP (3) recently derived [27] from the adiabatic theory [25] and confirmed in a previous experiment with atomic targets [26]. The SAE approximation with realistic molecular potentials was used for calculating the molecular properties needed to implement the factorization formula, namely, the DCSs, ionization rates, and TMD amplitudes. A good agreement in a wide range of laser intensities and scattering angles was achieved, illustrating the validity of the present theoretical method for the description of the strong-field ionization dynamics for molecular targets with unpaired (NO) as well as paired (CO) electrons in the HOMO. We also demonstrated the importance of taking into account the dependence of the RWP on the scattering angle. The advantage of having the analytical RWP enabled us to identify an effect of depletion of the initial state on the shape of the PEMD, particularly for higher laser intensities. The experimental and theoretical methods demonstrated in this work for diatomic molecules are expected to be applied in future studies to polyatomic molecules to obtain a deeper understanding of the rescattering processes.

ACKNOWLEDGMENTS

This work was supported in part by grants-in-aid for scientific research from the Japan Society for the Promotion of Science (JSPS); the X-ray Free Electron Laser Utilization Research Project and the X-ray Free Electron Laser Priority Strategy Program of the Ministry of Education, Culture, Sports, Science and Technology of Japan; the Dynamic Alliance for Open Innovation Bridging Human, Environment and Materials; IMRAM research program; and JSPS KAKENHI Grant No. 17K05739. T.M. was supported in part by JSPS KAKENHI Grants No. 16H04029, No. 16H04103, and No. 17K05597. O.I.T. acknowledges support from the Ministry of Education and Science of Russia (State Assignment No. 3.873.2017/4.6) and the Russian Foundation for Basic Research (Grant No. 17-02-00198).

[1] M. Ferray, A. L'Huillier, X. F. Li, L. A. Lompre, G. Mainfray, and C. Manus, Multiple-harmonic conversion of 1064 nm radiation in rare gases, J. Phys. B **21**, L31 (1988).

[2] B. Walker, B. Sheehy, L. F. DiMauro, P. Agostini, K. J. Schafer, and K. C. Kulander, Precision Measurement of Strong Field Double Ionization of Helium, Phys. Rev. Lett. **73**, 1227 (1994).

[3] B. Yang, K. J. Schafer, B. Walker, K. C. Kulander, P. Agostini, and L. F. DiMauro, Intensity-Dependent Scattering Rings in High Order Above-Threshold Ionization, Phys. Rev. Lett. **71**, 3770 (1993).

[4] G. G. Paulus, W. Nicklich, H. Xu, P. Lambropoulos, and H. Walther, Plateau in Above Threshold Ionization Spectra, Phys. Rev. Lett. **72**, 2851 (1994).

[5] P. B. Corkum, Plasma Perspective on Strong Field multiphoton ionization, Phys. Rev. Lett. **71**, 1994 (1993).

[6] T. Zuo, A. D. Bandrauk, and P. B. Corkum, Laser-induced electron diffraction: A new tool for probing ultrafast molecular dynamics, Chem. Phys. Lett. **259**, 313 (1996).

[7] M. Meckel, D. Comtois, D. Zeidler, A. Staudte, D. Pavičić, H. C. Bandulet, H. Pépin, J. C. Kieffer, R. Dörner, D. M. Villeneuve, and P. B. Corkum, Laser-induced electron tunneling and diffraction, Science **320**, 1478 (2008).

[8] T. Morishita, A.-T. Le, Z. Chen, and C. D. Lin, Accurate Retrieval of Structural Information from Laser-Induced Photoelectron and High-Order Harmonic Spectra by Few-Cycle Laser Pulses, Phys. Rev. Lett. **100**, 013903 (2008).

[9] M. V. Frolov, N. L. Manakov, and A. F. Starace, Analytic formulas for above-threshold ionization or detachment plateau spectra, Phys. Rev. A **79**, 033406 (2009).

[10] A. Čerkić, E. Hasović, D. B. Milošević, and W. Becker, High-order above-threshold ionization beyond the first-order born approximation, Phys. Rev. A **79**, 033413 (2009).

[11] O. I. Tolstikhin, T. Morishita, and S. Watanabe, Adiabatic theory of ionization of atoms by intense laser pulses: One-dimensional zero-range-potential model, Phys. Rev. A **81**, 033415 (2010).

[12] M. Okunishi, T. Morishita, G. Prümper, K. Shimada, C. D. Lin, S. Watanabe, and K. Ueda, Experimental Retrieval of Target Structure Information from Laser-Induced Rescattered Photoelectron Momentum Distributions, Phys. Rev. Lett. **100**, 143001 (2008).

[13] D. Ray, B. Ulrich, I. Bocharova, C. Maharjan, P. Ranitovic, B. Gramkow, M. Magrakvelidze, S. De, I. V. Litvinyuk, A.-T. Le, T. Morishita, C. D. Lin, G. G. Paulus, and C. L. Cocke, Large-Angle Electron Diffraction Structure in Laser-Induced Rescattering from Rare Gases, Phys. Rev. Lett. **100**, 143002 (2008).

[14] M. Okunishi, H. Niikura, R. R. Lucchese, T. Morishita, and K. Ueda, Extracting Electron-Ion Differential Scattering Cross Sections for Partially Aligned Molecules by Laser-Induced Rescattering Photoelectron Spectroscopy, Phys. Rev. Lett. **106**, 063001 (2011).

[15] C. Wang, M. Okunishi, R. R. Lucchese, T. Morishita, O. I. Tolstikhin, L. B. Madsen, K. Shimada, D. Ding, and K. Ueda, Extraction of electron-ion differential scattering cross sections for C_2H_4 by laser-induced rescattering photoelectron spectroscopy, J. Phys. B **45**, 131001 (2012).

[16] T. Morishita, T. Umegaki, S. Watanabe, and C. D. Lin, High-resolution spatial and temporal microscopy with intense-laser-induced rescattering electrons, J. Phys.: Conf. Ser. **194**, 012011 (2009).

[17] J. Xu, C. I. Blaga, A. D. DiChiara, E. Sistrunk, K. Zhang, Z. Chen, A.-T. Le, T. Morishita, C. D. Lin, P. Agostini, and L. F. DiMauro, Laser-Induced Electron Diffraction for Probing Rare Gas Atoms, Phys. Rev. Lett. **109**, 233002 (2012).

[18] C. I. Blaga, J. Xu, A. D. DiChiara, E. Sistrunk, K. Zhang, P. Agostini, T. A. Miller, L. F. DiMauro, and C. D. Lin, Imaging ultrafast molecular dynamics with laser-induced electron diffraction, Nature (London) **483**, 194 (2012).

[19] M. G. Pullen, B. Wolter, A.-T. Le, M. Baudisch, M. Hemmer, A. Senftleben, C. D. Schröter, J. Ullrich, R. Moshammer, C. D. Lin, and J. Biegert, Imaging an aligned polyatomic molecule with laser-induced electron diffraction, Nat. Commun. **6**, 7262 (2015).

[20] B. Wolter, M. G. Pullen, A.-T. Le, M. Baudisch, K. Doblhoff-Dier, A. Senftleben, M. Hemmer, C. D. Schroeter, J. Ullrich, T. Pfeifer, R. Moshammer, S. Graefe, O. Vendrell, C. D. Lin, and J. Biegert, Ultrafast electron diffraction imaging of bond breaking in di-ionized acetylene, Science **354**, 308 (2016).

[21] Y. Ito, C. Wang, A.-T. Le, M. Okunishi, D. Ding, C. D. Lin, and K. Ueda, Extracting conformational structure information of benzene molecules via laser-induced electron diffraction, Struct. Dyn. **3**, 034303 (2016).

[22] S. G. Walt, N. Bhargava Ram, M. Atala, N. I. Shvetsov-Shilovski, A. von Conta, D. Baykusheva, M. Lein, and H. J. Wörner, Dynamics of valence-shell electrons and nuclei probed by strong-field holography and rescattering, Nat. Commun. **8**, 15651 (2017).

[23] Y. Ito, R. Carranza, M. Okunishi, R. R. Lucchese, and K. Ueda, Extraction of geometrical structure of ethylene molecules by laser-induced electron diffraction combined with *ab initio* scattering calculations, Phys. Rev. A **96**, 053414 (2017).

[24] J. Xu, Z. Chen, A.-T. Le, and C. D. Lin, Self-imaging of molecules from diffraction spectra by laser-induced rescattering electrons, Phys. Rev. A **82**, 033403 (2010).

[25] O. I. Tolstikhin and T. Morishita, Adiabatic theory of ionization by intense laser pulses: Finite-range potentials, Phys. Rev. A **86**, 043417 (2012).

[26] H. Geiseler, N. Ishii, K. Kaneshima, F. Geier, T. Kanai, O. I. Tolstikhin, T. Morishita, and J. Itatani, Carrier-envelope phase mapping in laser-induced electron diffraction, Phys. Rev. A **94**, 033417 (2016).

[27] T. Morishita and O. I. Tolstikhin, Adiabatic theory of strong-field photoelectron momentum distributions near a backward rescattering caustic, Phys. Rev. A **96**, 053416 (2017).

[28] J. Wu, L. Ph. H. Schmidt, M. Kunitski, M. Meckel, S. Voss, H. Sann, H. Kim, T. Jahnke, A. Czasch, and R. Dörner, Multiorbital tunneling ionization of the CO molecule, Phys. Rev. Lett. **108**, 183001 (2012).

[29] B. Zhang, J. Yuan, and Z. Zhao, Dynamic core polarization in strong-field ionization of CO molecule, Phys. Rev. Lett. **111**, 163001 (2013).

[30] V. P. Majety and A. Scrinzi, Static field ionization rates for multi-electron atoms and small molecules, J. Phys. B **48**, 245603 (2015).

[31] A. R. Edmonds, *Angular Momentum in Quantum Mechanics* (Princeton University, Princeton, NJ, 1957).

[32] L. Hamonou, T. Morishita, and O. I. Tolstikhin, Molecular Siegert states in an electric field, Phys. Rev. A **86**, 013412 (2012).

[33] V. N. T. Pham, O. I. Tolstikhin, and T. Morishita, Molecular Siegert states in an electric field. II. Transverse momentum distribution of the ionized electrons, Phys. Rev. A **89**, 033426 (2014).

[34] R. H. Garvey, C. H. Jackman, and A. E. S. Green, Independent-particle-model potentials for atoms and ions with $36 < Z \leqslant 54$ and a modified Thomas-Fermi atomic energy formula, Phys. Rev. A **12**, 1144 (1975).

[35] J. Kobus, L. Laaksonen, and D. Sundholm, A numerical Hartree-Fock program for diatomic molecules, Comput. Phys. Commun. **98**, 346 (1996).

[36] O. I. Tolstikhin, T. Morishita, and L. B. Madsen, Theory of tunneling ionization of molecules: Weak-field asymptotics including dipole effects, Phys. Rev. A **84**, 053423 (2011).

[37] L. B. Madsen, O. I. Tolstikhin, and T. Morishita, Application of the weak-field asymptotic theory to the analysis of tunneling ionization of linear molecules, Phys. Rev. A **85**, 053404 (2012).

[38] R. Saito, O. I. Tolstikhin, L. B. Madsen, and T. Morishita, Structure factors for tunneling ionization rates of diatomic molecules, At. Data. Nucl. Data Tables **103–104**, 4 (2015).

[39] O. I. Tolstikhin, S. Watanabe, and M. Matsuzawa, 'Slow' variable discretization: A novel approach for Hamiltonians allowing adiabatic separation of variables, J. Phys. B **29**, L389 (1996).

[40] K. L. Baluja, P. G. Burke, and L. A. Morgan, *R*-matrix propagation program for solving coupled second-order differential equations, Comput. Phys. Commun. **27**, 299 (1982).

[41] O. I. Tolstikhin and H. Nakamura, Hyperspherical elliptic coordinates for the theory of light atom transfer reactions in atom-diatom collisions, J. Chem. Phys. **108**, 8899 (1998).

[42] Y. Zhou, S. Watanabe, O. I. Tolstikhin, and T. Morishita, Hyperspherical calculations of ultralow-energy collisions in Coulomb three-body systems, Phys. Rev. A **92**, 032713 (2015).

[43] S. Augst, D. D. Meyerhofer, D. Strickland, and S. L. Chin, Laser ionization of noble gases by Coulomb-barrier suppression, J. Opt. Soc. Am. B **8**, 858 (1991).

[44] T. Morishita, Z. Chen, S. Watanabe, and C. D. Lin, Two-dimensional electron momentum spectra of argon ionized by short intense lasers: Comparison of theory with experiment, Phys. Rev. A **75**, 023407 (2007).